Cation Distribution Tuning of Solution Combusted $CoFe_2O_4$ Powders

B. Pourgolmohammad, S. M. Masoudpanah* and M. R. Aboutalebi

* *masoodpanah@iust.ac.ir*

Received: September 2017 Accepted: February 2018

School of Metallurgy & Materials Engineering, Iran University of Science and Technology, Tehran, Iran.

DOI: 10.22068/ijmse.15.2.67

Abstract: *In this work, the different fuels (citric acid, glycine and urea) were used for solution combustion synthesis of $CoFe_2O_4$ powders. X-ray diffraction, Raman spectroscopy, electron microscopy and vibrating sample magnetometry techniques were employed for characterization of phase evolution, cation distribution, microstructure and magnetic properties of the as-combusted $CoFe_2O_4$ powders. Single phase $CoFe_2O_4$ powders with partially inverse structure in which the Co2+ cations are distributed in both tetrahedral and octahedral sites were synthesized by the citric acid, glycine and urea fuels. The as-combusted $CoFe_2O_4$ powders by the citric acid fuel exhibited the highest inversion coefficient. The crystallite size of the as-combusted $CoFe_2O_4$ powders synthesized by urea fuel was 15 nm, increased to 41 and 52 nm for the glycine and citric acid fuels, respectively. Furthermore, the solution combusted $CoFe_2O_4$ powders showed ferromagnetic behavior with saturation magnetization of 61.9, 63.6 and 41.6 emu/g for the citric acid, glycine and urea fuels, respectively. The high crystallinity and particle size of the as-combusted $CoFe_2O_4$ powders using glycine fuel led to the highest magnetization and the moderate coercivity.*

Keywords: *Fuel, Cation distribution, Inversion coefficient, Magnetic properties;*

1. INTRODUCTION

Cobalt ferrite ($CoFe_2O_4$) as a spinel magnetic ferrite has been considered as well-known material for electronic devices and magneto-optical recording media due to its moderate saturation magnetization and high magnetocrystalline anisotropy [1, 2]. High surface area $CoFe_2O_4$ powders with the excellent chemical stability and electrochemical properties have been found great potential applications in energy storage, catalysis, sensor, water purification, etc. [3-5].

Synthesis method strongly influences on magnetic, electrical and electrochemical properties of cobalt ferrite powders. Various synthesis methods such as hydrothermal, coprecipitation, thermal decomposition and solution combustion have been extensively applied for preparation of $CoFe_2O_4$ powders [6-9]. However, solution combustion synthesis (SCS) has been attracted a great attention for its simplicity, energy- and time-saving and environmentally friendliness [10]. SCS involves a redox reaction between oxidizer (metal salts such as nitrates, sulfates, carbonates, etc.) and fuel (usually urea, glycine, citric acid, etc.). The redox reaction initiates at moderate low temperatures (~150–200 °C). However, the released heat of combustion reaction leads to propagation of a rapid high temperature (1000–3000 °C) reaction wave in a self-sustained manner, causing the formation of solid product without any additional energy [11, 12]. The initial molecular level mixing of cations induced by complex formation helps to achieve a more homogeneous precursor which is beneficial for preparation multicomponent compounds such as superconductors, spinels, garnets, etc. [13]. The as-combusted products exhibit high porosity and high specific surface area due to the liberation of a large amount of gaseous products [13, 14]. However, powder characteristics such as phase, morphology, particle size and surface area are greatly dependent on fuel type, fuel/oxidizer ratio (ϕ), pH, salt additives, etc.[15-19]. For example, the amount of released gases products and combustion temperature are mainly related to the fuel characteristics such as solubility, decomposition temperature and reactivity [20]. Among of all types of fuel, the urea and glycine are popular fuels due to their high solubility in water, low decomposition temperature (< 400 °C), readily available and low cost [18]. The

[DOI: 10.22068/ijmse.15.2.67]

citric acid fuel has been attracted a great attention due to its high exothermicity and coordination ability [21]. Lazarova et al. [22] showed the as-combusted nickel ferrite powders using NH_2-contained fuels (e. g. urea and glycine) had the larger particle size and higher aggregation ability in comparison with pure carbohydrates fuels (e. g. glucose and sucrose).

In this work, we reported the role of the stoichiometric amount of various fuels (urea, glycine and citric) on phase evolution, cation distribution, microstructure and magnetic properties of the as-combusted $CoFe_2O_4$ powders. The distribution of Co^{2+} cations in tetrahedral and octahedral sites were dependent on fuel type which tuned the saturation magnetization.

2. EXPERIMENTAL PROCEDURE

The precursor of $Fe(NO_3)_3.9H_2O$), cobalt nitrate ($Co(NO_3)_2.6H_2O$), glycine (NH_2CH_2COOH), urea ($CO(NH_3)_2$) and citric acid ($C_6H_8O_7$) were purchased from Merck Co..

The required amounts of ferric nitrate ($Fe(NO_3)_3.9H_2O$), cobalt nitrate ($Co(NO_3)_2.6H_2O$) and fuel were dissolved in the distilled water. The fuels were glycine (NH_2CH_2COOH), urea ($CO(NH_3)_2$) and citric acid ($C6H_8O_7$) which were used at fuel to oxidant ratio of 1 (ϕ=1). After homogenization, the mixture was poured into a dish and heated till to transform into a gel and ignited by further heating up to 250 °C on a hot plate. The resulted powders were hand-crushed with a pestle.

Raman analysis was performed on powders by WiTec Alpha 300R instrument (Nd:YAG laser source: λ = 532 nm and 0.7 Mw power, and range: 100–900 cm^{-1}).

Phase evolution was analyzed by PANalytical X-ray diffractometer (XRD) using monochromatic CuKα radiation. The average crystallite size was also calculated from the width (311) peak using Scherrer's equation. The morphology and microstructure of the powders were observed by TESCAN Vega II field emission scanning electron microscopy.

A vibrating sample magnetometer (Meghnatis Daghigh Kavir Co., Iran) was also employed to measure the magnetic properties of cobalt ferrite powders at room temperature.

All of the thermodynamic calculations in this research were performed using the FactSage 6.1 software [23].

3. RESULTS AND DISCUSSION

The redox processes for stoichiometric mixture that are taking place during combustion reaction can be written according to Eqs. (1) to (3):

$$Co(NO_3)_2 + 2Fe(NO_3)_3 + \frac{20}{9}C_6H_8O_7 \rightarrow CoFe_2O_4 + \frac{40}{3}CO_2 + \frac{80}{9}H_2O + 4N_2 \quad (1)$$

$$Co(NO_3)_2 + 2Fe(NO_3)_3 + \frac{40}{9}C_2H_5NO_2 \rightarrow CoFe_2O_4 + \frac{80}{9}CO_2 + \frac{100}{9}H_2O + \frac{56}{9}N_2 \quad (2)$$

$$Co(NO_3)_2 + 2Fe(NO_3)_3 + \frac{40}{6}CH_4N_2O \rightarrow CoFe_2O_4 + \frac{40}{6}CO_2 + \frac{40}{3}H_2O + \frac{64}{6}N_2 \quad (3)$$

The stoichiometric mixture does not require atmospheric oxygen for complete fuel oxidation, leading to the maximum adiabatic combustion temperature [13, 24]. The adiabatic combustion temperature (T_{ad}) were calculated by FactSage software for synthesis of cobalt ferrite. The maximum adiabatic combustion temperature is 1796, 1668 and 1537 K using citric acid, glycine and urea fuels, respectively [25].

XRD patterns of the as-combusted $CoFe_2O_4$ powders using citric acid, glycine and urea fuels are shown in Fig. 1. The indexed peaks as (220), (311), (222), (400), (422), (511) and (440) of the cubic spinel structure confirm the direct formation of single phase $CoFe_2O_4$ after combustion reaction without further heat treatment. The wider and noisy diffraction peaks for urea fuel are due to its small crystallite size and lower crystallinity originated from lower adiabatic temperature. Furthermore, the weak coordination ability of glycine fuel results in

[DOI: 10.22068/ijmse.15.2.67]

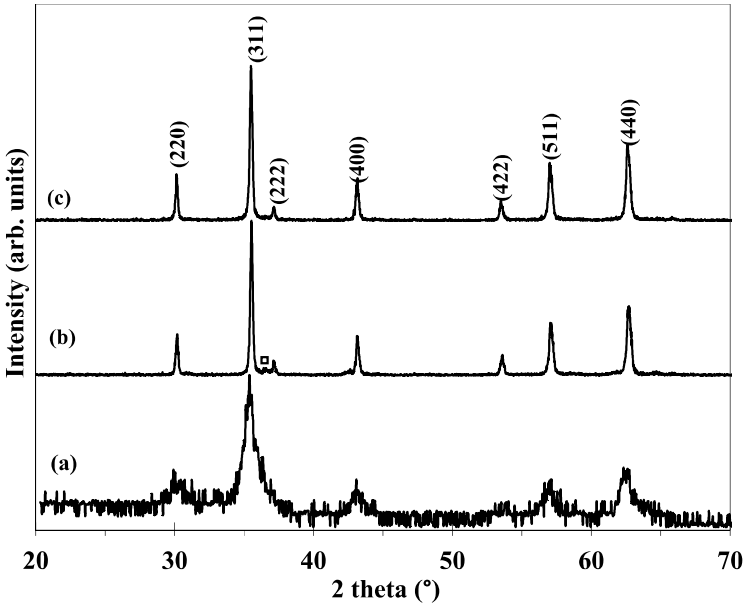

Fig. 1. XRD patterns of the as-combusted $CoFe_2O_4$ powders using (a) urea, (b) glycine and (c) citric acid fuels (□:CoO).

Table 1. Cation distribution and crystallite size of the as-combusted $CoFe_2O_4$ as a function of fuel type.

Fuel	I220/I400		I422/I400		Cation distribution	Crystallite size (nm)
	Obs.	Calc.	Obs.	Calc.		
Urea	1.10	1.26	0.11	0.21	$(Co_{0.09}Fe_{0.91})_A[Co_{0.09}Fe_{1.91}]_BO_4$	15
Glycine	1.21	1.31	0.31	0.39	$(Co_{0.05}Fe_{0.95})_A[Co_{0.95}Fe_{1.05}]_BO_4$	41
Citric acid	1.65	1.71	0.35	0.42	$(Co_{0.03}Fe_{0.97})_A[Co_{0.97}Fe_{1.03}]_BO_4$	52

some impurity CoO phase. The crystallite size of the as-combusted $CoFe_2O_4$ powders using urea fuel is 15 nm, increases to 41 and 52 nm for glycine and citric acid fuels, respectively, as listed in Table 1. The higher crystallite sizes using citric acid fuel can be attributed to its higher adiabatic combustion temperature.

The cation distribution can be determined by analyzing of XRD patterns by Bertaut method [26]. This method compares the observed intensity ratios with the calculated intensity ratios for exploring the minimum of agreement factor (R) by varying the cation distribution in the supposed structure [27]:

$$R = \left(\frac{I_{hkl}}{I_{\acute{h}\acute{k}\acute{l}}}\right)_{Obs.} - \left(\frac{I_{hkl}}{I_{\acute{h}\acute{k}\acute{l}}}\right)_{Calc.} \quad (4)$$

The relative integrated intensity of a given diffraction line from powder specimens in a diffractometer with a flat plate sample holder can be calculated by following formula [28]:

$$I_{hkl} = |F_{hkl}|^2 P L_p \quad (5)$$

which P is the multiplicity factor and L_p is the Lorenz-polarization factor which depends only on Bragg's diffraction angle θ, as follows [29]:

$$L_p = \frac{1+cos^2 2\theta}{sin^2\theta cos2\theta} \quad (6)$$

and F_{hkl} is the structure factor which can be described for 220, 400 and 422 planes as follows [30]:

[DOI: 10.22068/ijmse.15.2.67]

$$F_{220} = -8F_A + 16f_O(cos8\pi u - 1) \quad (7)$$

$$F_{400} = 8(F_A - F_B + 4f_O cos8\pi u) \quad (8)$$

$$F_{422} = -8F_A + 8f_O(cos16\pi u - 2cos8\pi u + 1) \quad (9)$$

which u is oxygen positional parameter, fO is scattering factor of oxygen atom and FA and FB are the total scattering factor of atoms in A- and B-sites, respectively. For $(Co_{1-\delta}Fe_{\delta})_A[Co_{\delta}Fe_{2-\delta}]_BO_4$, F_A and F_B can be written as:

$$F_A = (1-\delta)f_{Co} + \delta f_{Fe} \quad (10)$$

$$F_B = \delta f_{Co} + (2-\delta)f_{Fe} \quad (11)$$

which f_{Co} and f_{Fe} are scattering factors of cobalt and iron atoms, respectively. The thermal correction of diffraction line is no need for spinel structure on account of its high melting point [29]. Some peaks' intensity ratios like I220/I400, I220/I422 and I422/I400 as cation distribution sensitive peaks can be used for determination of the cation distribution in spinel structures [28]. The cation distributions as a function of fuel type are given in Table 1. Cation distribution shows that the as-combusted $CoFe_2O_4$ powders have a partially inverse structure in which the divalent cations (Co^{2+}) are distributed in tetrahedral (A) and octahedral [B] sites. The inversion coefficient (δ) defined as the fraction of Fe^{3+} cations in tetrahedral sites (A-sites) depends on fuel type. The highest inversion coefficient (δ=0.97) for citric acid fuel can be attributed to the higher chelatability and adiabatic combustion temperature which promote the cation diffusion.

The theoretical lattice parameter can be calculated by following equation [31]:

$$a_{th} = \frac{8}{3\sqrt{3}}\left[(r_A + R_O) + \sqrt{3}(r_B + R_O)\right] \quad (12)$$

where r_A and r_B are the radii of tetrahedral and octahedral sites and R_O is the radius of oxygen ions (R_O=1.32 Å). The mean ionic radius of tetrahedral (A) and octahedral [B] sites (r_A and r_B) can be calculated by following relations [31]:

$$r_A = (1-\delta)r_{Co^{2+}} + \delta r_{Fe^{3+}} \quad (13)$$

$$r_B = \frac{1}{2}[\delta r_{Co^{2+}} + (2-\delta)r_{Fe^{3+}}] \quad (14)$$

The radii of tetrahedral and octahedral sites and theoretical (a_{th}) and experimental (a_{exp}) lattice parameters are presented in Table 2. The agreement between a_{th} and a_{exp} indirectly verifies the cation distribution deduced from X-ray intensity calculations [32].

Raman spectra of the as-combusted $CoFe_2O_4$ powders in the range of 100–800 cm^{-1} are shown in Fig. 2. The irreducible representations for spinel ferrite structures with O7h (Fd3m) space group are as follows [33]:

$$\Gamma_{irred} = A_{1g}(R) + Eg(R) + T_{1g} + 3T_{2g}(R) + 2A_{2u} + 2E_u + T_{1u}(IR) + 2T_{2u} \quad (15)$$

The $A_{1g}(R)+E_g(R)+3T_{2g}(R)$ modes are Raman active modes at ambient conditions and the T_{1u} is only infrared active mode. The T_{1g}, A_{2u}, Eu and T_{2u} are silent symmetry vibration modes. The natural frequency of the Raman active modes was determined by a least square fit with Lorentzian line shape, as illustrated in Fig. 2. Table 3 presents the Raman shifts and their assignments of the as-combusted $CoFe_2O_4$ powders as a function of fuel type. The broadening of the high

Table 2. The average ionic radius of the tetrahedral and octahedral sites (rA and rB) and experimental (aexp) and theoretical (ath) lattice parameter.

Fuel	r_A (Å)	r_B (Å)	a_{exp} (Å)	$a_{th.}$(Å)
Urea	0.654	0.6905	8.3930	8.4003
Glycine	0.65	0.6925	8.3830	8.3995
Citric acid	0.648	0.6935	8.3983	8.3991

[DOI: 10.22068/ijmse.15.2.67]

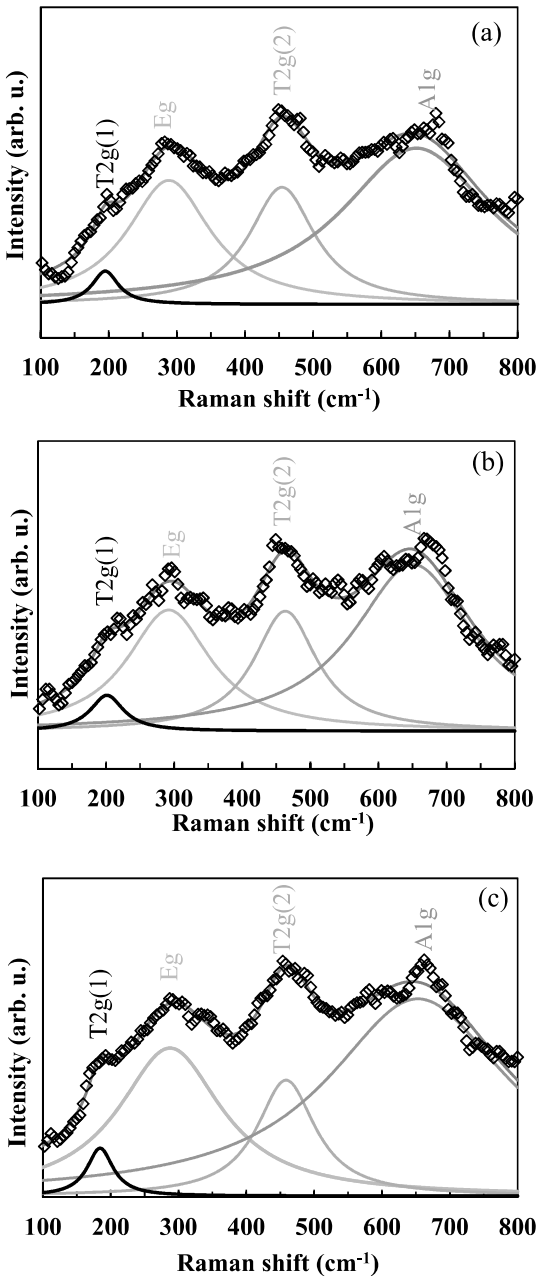

Fig. 2. Raman spectra of the as-combusted $CoFe_2O_4$ powders using (a) urea, (b) glycine and (c) citric acid fuels.

frequency modes due to the small crystallite size of $CoFe_2O_4$ powders eliminates low-frequency modes. The motion of oxygen in tetrahedral AO_4 group (A-site) leads to Raman shifts above 600 cm^{-1}, while the other low Raman shifts are related to the octahedral BO_6 group (B-site) [34]. All

Table 3. Raman parameters of the as-combusted $CoFe_2O_4$ powders.

Fuel	Assignment			
	T2g(1)	Eg	T2g(2)	A1g
Urea	194	288	458	653
Glycine	201	291	463	650
Citric acid	184	285	451	649

modes of the as-combusted $CoFe_2O_4$ powders using citric acid fuel are shifted toward the lower wave number region, may be due to its highest inversion coefficient.

The microstructures of as-combusted $CoFe_2O_4$ powders using citric acid, glycine and urea fuels are shown in Fig. 3. For urea fuel, the particles are tightly agglomerated in the range of 5 and 20 μm. The increase of pH by decomposition of urea induces the precipitation of hydroxides, which aggregate during combustion reaction [18]. However, the particles were sintered using glycine fuel, due to its fast thermal decomposition. The bulky morphology of the as-combusted $CoFe_2O_4$ powders using citric acid fuel can be attributed to the establishment of polymeric network between the citrate species, postponing the liberation of gaseous products. It was also reported the COOH ligand has lower reactivity than that of $–NH_2$ group for releasing gaseous products, leading to the bulky microstructure of the as-combusted powders using citric acid fuel [20].

Fig. 4 shows the magnetization curves of the as-combusted $CoFe_2O_4$ powders by various fuels at ϕ=1. The saturation magnetization (Ms), remanence (Mr) and coercivity (Hc) values are presented in Table 4. The as-combusted $CoFe_2O_4$ powders using glycine fuel exhibit the highest saturation magnetization (63.9 emu/g), in spite of

Table 4. Magnetic properties of the as-combusted $CoFe_2O_4$ powders

Fuel	Ms (emu/g)	Mr (emu/g)	Hc (Oe)
Urea	41.6	11.8	847
Glycine	63.6	32.5	1113
Citric acid	61.9	27.4	1335

[DOI: 10.22068/ijmse.15.2.67]

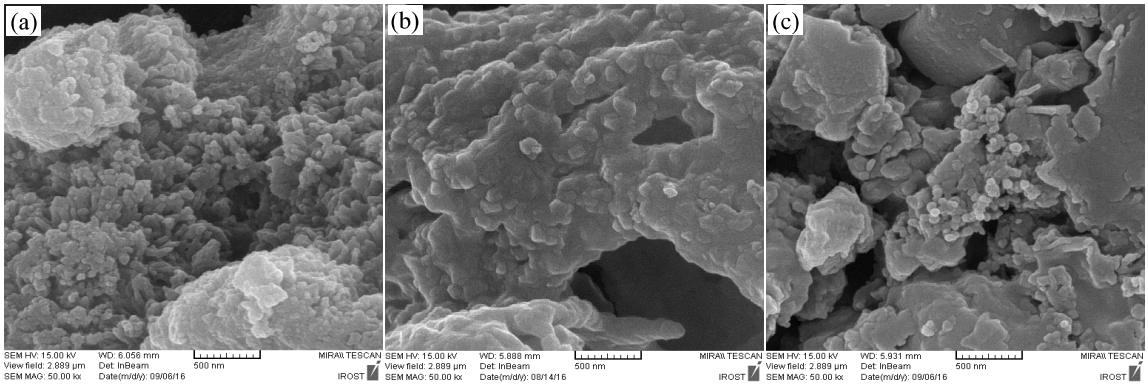

Fig. 3. SEM micrographs of the as-combusted $CoFe_2O_4$ powders using (a) urea, (b) glycine and (c) citric acid fuels

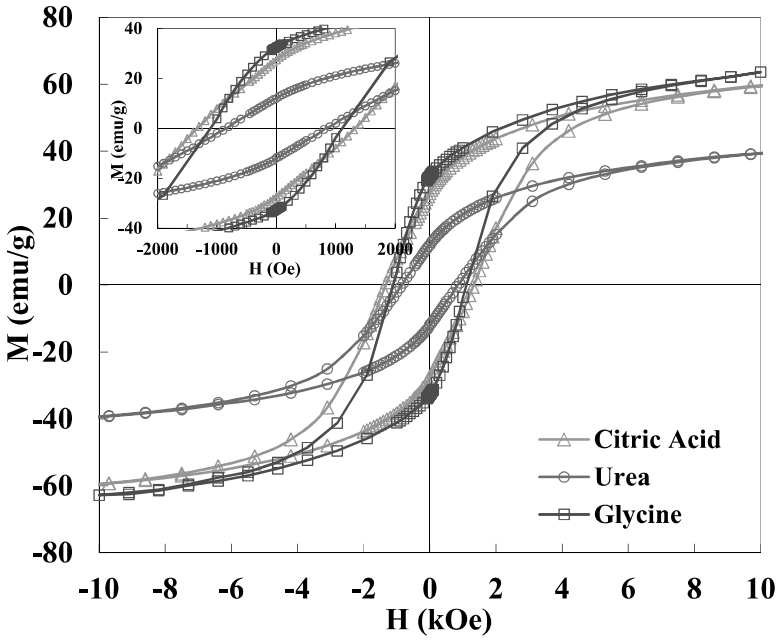

Fig. 4. Hysteresis loops of the as-combusted $CoFe_2O_4$ powders using different fuels.

some impure CoO phase. This can be attributed to the higher crystallinity originated from higher combustibility of glycine [13]. In spite of the higher purity and adiabatic temperature for citric acid fuel, the saturation magnetization is slightly lower than that for glycine fuel, may be due to its highest inversion coefficient. The cubic spinel ferrites have two different sublattices for magnetic ions, i.e., tetrahedral (A) and octahedral [B] sublattices. The superexchange interaction between the magnetic ions in the A and B sublattices controls the magnetic order in magnetic spinel ferrite. According to the Neel model, A–B superexchange interactions are predominant over intrasublattice A–A and B–B interactions and the saturation magnetization is given by the vector sum of the net magnetic moments of the individual A and B sublattices [35]. The more Fe^{3+} cations with the ionic magnetic moments of $5_{\mu B}$ in tetrahedral (A) sites

[DOI: 10.22068/ijmse.15.2.67]

in the higher inversity decreases the magnetic moment of the B-site and then the total magnetic moments.

The lowest Hc of 847 Oe is obtained for the urea fuel, because their crystallite size is smaller than that of single-domain size limit (~ 40 nm). The prevailing of the thermal energy on the anisotropy energy for D<40 nm leads to the decrease of Hc [36,37]. The solution combusted $CoFe_2O_4$ powders usually exhibit the higher saturation magnetization in comparison with the other synthetic methods due to their high crystallinity originated from high adiabatic combustion temperature. However, the coercivity is strongly related to the particle size, making the comparison difficult.

4. CONCLUSION

Single phase $CoFe_2O_4$ powders have been prepared by solution combustion method using urea, glycine and citric acid as fuel. The cation distribution in tetrahedral and octahedral sites determined by XRD analysis was strongly dependent on fuel type. The higher coordination ability of citric acid toward cations resulted in the highest inversion coefficient. The sintered microstructure of the as-combusted $CoFe_2O_4$ powders using glycine fuel was attributed to its fast combustion and high adiabatic temperature. Furthermore, the magnetic properties of the as-combusted $CoFe_2O_4$ powders can be adjusted by the fuel type through crystallinity, crystallite size and cation distribution.

REFERENCES

1. Zhang, D.; Pu, X.; Gao, Y.; Su, C.; Li, H.; Li, H.; Hang, W. "One-step combustion synthesis of $CoFe_2O_4$–graphene hybrid materialsfor photodegradation of methylene blue". Materials Letters, 2013, 113, 179-181.
2. Hou, Y. H., Huang, Y. L., Hou, S. J., Ma, S. C., Liu, Z. W., Ouyang, Y. F., "Structural, electronic and magnetic properties of RE^{3+}-doping in $CoFe_2O_4$: A first-principles study". Journal of Magnetism and Magnetic Materials, 2017, 421, 300-305.
3. Rai, A. K., Gim, J., Thi, T. V., Ahn, D., Cho, S. J., Kim, J., "High Rate Capability and Long Cycle Stability of $Co_3O_4/CoFe_2O_4$ Nanocomposite as an Anode Material for High-Performance Secondary Lithium Ion Batteries". The Journal of Physical Chemistry C, 2014, 118, 11234-11243.
4. Li, N., Zheng, M., Chang, X., Ji, G., Lu, H., Xue, L., Pan, L., Cao, J., "Preparation of magnetic $CoFe_2O_4$-functionalized graphene sheets via a facile hydrothermal method and their adsorption properties". Journal of Solid State Chemistry, 2011, 184, 953-958.
5. Reddy, D. H. K., Yun, Y. S., "Spinel ferrite magnetic adsorbents: Alternative future materials for water purification", Coordination Chemistry Reviews, 2016, 315, 90-111.
6. Millot, N., Le Gallet, S., Aymes, D., Bernard, F., Grin, Y., "Spark plasma sintering of cobalt ferrite nanopowders prepared by coprecipitation and hydrothermal synthesis". Journal of the European Ceramic Society, 2007, 27, 921-926.
7. Reddy, M. P., Mohamed, A. M. A., Zhou, X. B., Du, S., Huang, Q., "A facile hydrothermal synthesis, characterization and magnetic properties of mesoporous $CoFe_2O_4$ nanospheres". Journal of Magnetism and Magnetic Materials, 2015, 388, 40-44.
8. Houshiar, M., Zebhi, F., Razi, Z. J., Alidoust, A., Askari, Z., "Synthesis of cobalt ferrite ($CoFe_2O_4$) nanoparticles using combustion, coprecipitation, and precipitation methods: A comparison study of size", structural, and magnetic properties. Journal of Magnetism and Magnetic Materials, 2014, 371, 43-48.
9. Pourgolmohammad, B., Masoudpanah, S. M., Aboutalebi, M. R., "Effects of the fuel type and fuel content on the specific surface area and magnetic properties of solution combusted $CoFe_2O_4$ nanoparticles". Ceramics International, 2017, 43, 8262-8268.
10. Wen, W., Wu, J. M., "Nanomaterials via solution combustion synthesis: a step nearer to controllability". RSC Advances, 2014, 4, 58090-58100.
11. Aruna, S. T., Mukasyan, A. S., "Combustion synthesis and nanomaterials". Current Opinion in Solid State and Materials Science, 2008, 12, 44-50.
12. Mukasyan, A. S., Rogachev, A. S., Aruna, S. T.,

[DOI: 10.22068/ijmse.15.2.67]

"Combustion synthesis in nanostructured reactive systems. Advanced Powder Technology", 2015, 26, 954-976.
13. Varma, A., Mukasyan, A. S., Rogachev, A. S., Manukyan, K. V., "Solution Combustion Synthesis of Nanoscale Materials". Chemical Reviews, 2016, 116, 14493-14586.
14. Manukyan, K. V., Chen, Y. S., Rouvimov, S., Li, P., Li, X., Dong, S., Liu, X., Furdyna, J. K., Orlov, A., Bernstein, G. H., Porod, W., Roslyakov, S., Mukasyan, A. S., "Ultrasmall α-Fe_2O_3 Superparamagnetic Nanoparticles with High Magnetization Prepared by Template-Assisted Combustion Process". The Journal of Physical Chemistry C, 2014, 118, 16264-16271.
15. Pourgolmohammad, B., Masoudpanah, S. M., Aboutalebi, M. R., "Effect of starting solution acidity on the characteristics of $CoFe_2O_4$ powders prepared by solution combustion synthesis". Journal of Magnetism and Magnetic Materials, 2017, 424, 352-358.
16. Zhang, X., Jiang, W., Song, D., Sun, H., Sun, Z., Li, F., "Salt-assisted combustion synthesis of highly dispersed superparamagnetic $CoFe_2O_4$ nanoparticles". Journal of Alloys and Compounds, 2009, 475, L34-L37.
17. Parnianfar, H., Masoudpanah, S. M., Alamolhoda, S., Fathi, H., "Mixture of fuels for solution combustion synthesis of porous Fe_3O_4 powders". Journal of Magnetism and Magnetic Materials, 2017, 432, 24-29.
18. Fathi, H., Masoudpanah, S. M., Alamolhoda, S., Parnianfar, H., "Effect of fuel type on the microstructure and magnetic properties of solution combusted Fe_3O_4 powders". Ceramics International, 2017, 43, 7448-7453.
19. Chen, W.; Li, F.; Yu, J.; Liu, L. A facile and novel route to high surface area ceria-based nanopowders by salt-assisted solution combustion synthesis. Materials Science and Engineering: B, 2006, 133, 151-156.
20. Erri, P., Pranda, P., Varma, A., "Oxidizer−Fuel Interactions in Aqueous Combustion Synthesis". 1. Iron(III) Nitrate−Model Fuels. Industrial & Engineering Chemistry Research, 2004, 43, 3092-3096.
21. Radpour, M., Masoudpanah, S. M., Alamolhoda, S., "Microwave-assisted solution combustion synthesis of Fe_3O_4 powders". Ceramics International.
22. Lazarova, T., Georgieva, M., Tzankov, D., Voykova, D., Aleksandrov, L., Cherkezova-Zheleva, Z., Kovacheva, D., "Influence of the type of fuel used for the solution combustion synthesis on the structure, morphology and magnetic properties of nanosized $NiFe_2O_4$". Journal of Alloys and Compounds, 2017, 700, 272-283.
23. Bale, C. W., Bélisle, E., Chartrand, P., Decterov, S. A., Eriksson, G., Hack, K., Jung, I. H., Kang, Y. B., Melançon, J., Pelton, A. D., Robelin, C., Petersen, S., "FactSage thermochemical software and databases — recent developments". Calphad, 2009, 33, 295-311.
24. Nersisyan, H. H., Lee, J. H., Ding, J. R., Kim, K. S., Manukyan, K. V., Mukasyan, A. S., "Combustion synthesis of zero-, one-, two- and three-dimensional nanostructures: Current trends and future perspectives". Progress in Energy and Combustion Science, 2017, 63, 79-118.
25. Cox, J., Wagman, D. D., Medvedev, V. A., "CODATA key values for thermodynamics", Chem/Mats-Sci/E, 1989.
26. Aliyan, N., Mirkazemi, S. M., Masoudpanah, S. M., Akbari, S., "The effect of post-calcination on cation distributions and magnetic properties of the coprecipitated $MgFe_2O_4$ nanoparticles". Applied Physics A, 2017, 123, 446.
27. Najmoddin, N., Beitollahi, A., Kavas, H., Majid Mohseni, S., Rezaie, H., Åkerman, J., Toprak, M. S., "XRD cation distribution and magnetic properties of mesoporous Zn-substituted $CuFe_2O_4$". Ceramics International, 2014, 40, 3619-3625.
28. Skolnick, L. P., Kondo, S., Lavine, L. R., "An Improved X-Ray Method for Determining Cation Distribution in Ferrites". Journal of Applied Physics, 1958, 29, 198-203.
29. Cullity, B. D.: Elements of X-Ray Diffraction; Addison-Wesley: Boston, 1956.
30. Hasheminiasari, M., Masoudpanah, S. M., Mirkazemi, S. M., Bayat, F., "Structural and magnetic properties of $ZnFe_{2-x}InxO_4$ nanoparticles synthesized by solution combustion method". Journal of Magnetism and Magnetic Materials, 2017, 442, 468-473.
31. Sickafus, K. E., Wills, J. M., Grimes, N. W.,

[DOI: 10.22068/ijmse.15.2.67]

"Structure of Spinel". Journal of the American Ceramic Society, 1999, 82, 3279-3292.

32. Zaki, H. M., Al-Heniti, S., Al Shehri, N., "New scheme for cation distribution and electrical characterization of nanocrystalline aluminum doped magnesium ferrite $MgAlxFe_{2-x}O_4$". Physica B: Condensed Matter, 2014, 436, 157-163.
33. Wang, Z., Schiferl, D., Zhao, Y., O'Neill, H. S. C., "High pressure Raman spectroscopy of spinel-type ferrite $ZnFe_2O_4$". Journal of Physics and Chemistry of Solids, 2003, 64, 2517-2523.
34. Masoudpanah, S. M., Hasheminisari, M.; Ghasemi, A., "Magnetic properties and photocatalytic activity of $ZnFe_{2-x}$ La x O_4 nanoparticles synthesized by sol–gel autocombustion method". Journal of Sol-Gel Science and Technology, 2016, 80, 487-494.
35. Cullity, B. D., Graham, C. D., "Introduction to magnetic materials", John Wiley & Sons: New Jersay, 2011.
36. Spaldin, N. A., "Magnetic materials, fundamentals and applications," Cambridge University Press, 2010.
37. Goldman, A., "Modem Ferrite Technology", 2 ed.; Springer: Pittsburgh, PA, USA, 2006.

[DOI: 10.22068/ijmse.15.2.67]